Well-balanced path-consistent finite volume EG schemes for the two-layer shallow water equations

M. Dudzinski and M. Lukáčová-Medviďová

Abstract We present a new path-consistent well-balanced finite volume method within the framework of the evolution Galerkin (FVEG) schemes. The methodology will be illustrated for two layer shallow water equations with source terms modelling the bottom topography and Coriolis forces. The FVEG methods couple a finite volume formulation with approximate evolution operators. The latter are constructed using the bicharacteristics of multidimensional hyperbolic systems, such that all of the infinitely many directions of wave propagation are taken into account explicitly. We will derive a suitable path in the phase space that is based on the evolution operator and derive the corresponding path-consistent FVEG scheme. The path-consistent FVEG scheme is well-balanced for the stationary steady states as well as for the steady jets in the rotational frame.

1 Mathematical model

Many types of flows, not necessarily involving water, can be described as shallow water flows. Such flows are all characterized by negligible vertical scales in comparison to horizontal scales. Typical examples are rivers with their flood plains, flows in lakes generated by wind blows, propagation of tsunamis, oceanographic, meteorological and geophysical flows. For smooth flows different methods, such as finite difference schemes, finite element methods, or spectral methods perform quite well. Under some assumptions flows may exhibit discontinuities, such as tidal bores observed in some rivers, the wave resulting from the bursting of a dam or hydraulic jump in jets. In this situation, a moving step front develops, which is comparable to a shock wave in aerodynamics. In this work we consider the two-layer shallow water equations describing motion of immiscible inviscid fluids of constant density. This

Institute of Numerical Simulation, Hamburg University of Technology, Schwarzenbergstrasse 95, 21073 Hamburg e-mail: michael.dudzinski, lukacova@tu-harburg.de

type of flow appears, typically, in oceanographic models when a warm and light upper layer flows over a lower layer of cooler, heavier water with larger salinity.

Taking into account effects of the variable bottom topography and the Coriolis forces due to the earth rotation the system of two-layer shallow water equations can be formulated as follows

$$\begin{cases} \partial_t h_1 + \partial_x(h_1u_1) + \partial_y(h_1v_1) &= 0, \\ \partial_t(h_1u_1) + \partial_x\left(h_1u_1^2 + \frac{g}{2}h_1^2\right) + \partial_y(h_1u_1v_1) &= -gh_1\partial_x(b+h_2) - fh_1v_1, \\ \partial_t(h_1v_1) + \partial_x(h_1u_1v_1) + \partial_y\left(h_1v_1^2 + \frac{g}{2}h_1^2\right) &= -gh_1\partial_y(b+h_2) + fh_1u_1, \\ \partial_t h_2 + \partial_x(h_2u_2) + \partial_y(h_2v_2) &= 0, \\ \partial_t(h_2u_2) + \partial_x\left(h_2u_2^2 + \frac{g}{2}h_2^2\right) + \partial_y(h_2u_2v_2) &= -gh_2\partial_x(b+rh_1) - fh_2v_2, \\ \partial_t(h_2v_2) + \partial_x(h_2u_2v_2) + \partial_y\left(h_2v_2^2 + \frac{g}{2}h_2^2\right) &= -gh_2\partial_y(b+rh_1) + fh_2u_2. \end{cases} \tag{1}$$

Here h_1, h_2 denote the height of the corresponding layer, u_i and v_i are the vertically averaged velocities in the x- and y-direction, respectively, $i = 1,2$. Furthermore b is the time independent bottom topography, g the gravitational constant, f the Coriolis parameter and $r = \rho_1/\rho_2$ describes the effect of different constant densities $\rho_1 < \rho_2$.

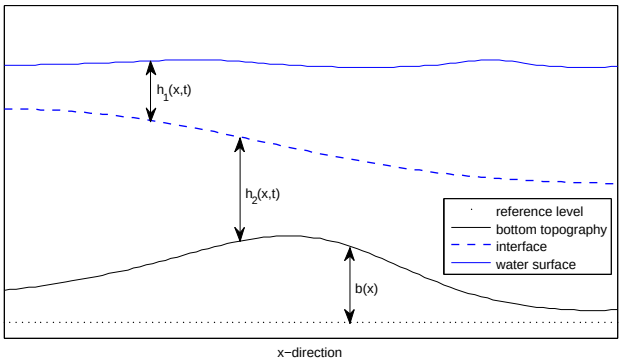

Fig. 1 Two shallow layers

Mathematically there are several challenging problems arising by numerical solution of the system (1). Indeed, we have non-conservative product terms, the system is only conditionally hyperbolic, nonstrictly hyperbolic, and its eigenstructure cannot be obtained in explicit form. In the literature several approaches to attack these problems [1], [2], [7] can be found.

Typically large scale flow in the ocean and the atmosphere is characterized by an approximate balance in the vertical direction between pressure gradient and gravity (hydrostatic balance), and in the horizontal direction between the pressure gradient and the Coriolis forces that arise due to the earth rotation (geostrophic balance).

Numerical scheme preserving important physical equilibria are called *well-balanced* schemes. In this paper the following fundamental equilibrium states will be considered

1. rest state (lake at rest):

$$h_1 + h_2 + b = \text{const.}, rh_1 + h_2 + b = \text{const.}, u_1 = v_1 = 0 = u_2 = v_2; \quad (2)$$

2. geostrophic equilibrium (jet in the rotational frame):

$$\begin{aligned} &g\partial_x(h_1+h_2+b) = -fv_1, u_1 = 0, g\partial_y(h_1+h_2+b) = 0, \partial_y v_1 = 0, v_1\partial_y h_1 = 0, \\ &g\partial_x(rh_1+h_2+b) = -fv_2, u_2 = 0, g\partial_y(rh_1+h_2+b) = 0, \partial_y v_2 = 0, v_2\partial_y h_2 = 0. \end{aligned} \quad (3)$$

Note that the condition (3) actually states the balance between the Coriolis forces and the pressure gradient in each layer; we assume here additionally that the flow is quasi one-dimensional, thus the y-derivatives are set to zero.

In our previous works [9], [10] we have developed the so-called *well-balanced finite volume evolution Galerkin scheme* for the one-layer shallow water system with bottom topography and the Coriolis forces. The scheme has been shown to be simple, accurate and surprisingly efficient. The finite volume evolution Galerkin schemes can be formulated as two-step predictor-corrector scheme. The first step, called predictor step, evolves the value at a quadrature node to the half-timestep. This has been done by fully multidimensional bicharacteristic theory, cf. [10]. The second step is the standard finite volume update. It approximates the flux integral across the interfaces by a quadrature of the fluxes evaluated at the predicted states at the half time step. Now in order to preserve equilibrium states, it is necessary to satisfy equilibrium conditions at both time steps. Let us note that in [10] we have approximated the right-hand-side source terms by the so-called cell-interface approach that exactly balances flux integrals.

On the other hand, there have been several interesting results presented recently in the literature where the non-conservative character of the right-hand-side source terms of (1) was taken into account. In order to define the concept of the weak solutions the theory developed by Dal Maso et al. [3] has been used. The most important point is to give an interpretation to the nonconservative products as Borel measures that are based on the choice of a family of paths drawn in the phase space. The concept of path-conservative or path-consistent numerical schemes has been introduced by Pares and Castro in [12], see also [11, 4, 6] and the references therein.

The goal of the present paper is two-fold: firstly we will derive a new well-balanced path-consistent finite volume evolution Galerkin method and secondly we apply this method for the two-layer shallow water equations.

2 Operator splitting technique

Let us firstly rewrite (1) in the quasi-linear form. Setting $\mathbf{W} = (\mathbf{w}_1, \mathbf{w}_2, b, x, y)^T$ and denoting conservative variables of the corresponding layer by $\mathbf{w}_i = (h_i, h_i u_i, h_i v_i)^T$, $i = 1, 2$, we obtain

$$\mathbf{W}_t + \widetilde{\mathbf{A}}_1(\mathbf{W})\mathbf{W}_x + \widetilde{\mathbf{A}}_2(\mathbf{W})\mathbf{W}_y = 0, \tag{4}$$

where

$$\widetilde{\mathbf{A}}_1 = \begin{pmatrix} \mathbf{A}_1(\mathbf{w}_1) & \mathbf{C}_1(\mathbf{w}_1) & -\mathbf{S}_1(\mathbf{w}_1) & -\mathbf{S}_3(\mathbf{w}_1) & 0 \\ \widetilde{\mathbf{C}}_1(\mathbf{w}_2) & \mathbf{A}_1(\mathbf{w}_2) & -\mathbf{S}_1(\mathbf{w}_2) & -\mathbf{S}_3(\mathbf{w}_2) & 0 \\ 0 & 0 & 0 & 0 & 0 \\ 0 & 0 & 0 & 0 & 0 \\ 0 & 0 & 0 & 0 & 0 \end{pmatrix},$$

$$\widetilde{\mathbf{A}}_2 = \begin{pmatrix} \mathbf{A}_2(\mathbf{w}_1) & \mathbf{C}_2(\mathbf{w}_1) & -\mathbf{S}_2(\mathbf{w}_1) & 0 & -\mathbf{S}_4(\mathbf{w}_1) \\ \widetilde{\mathbf{C}}_2(\mathbf{w}_2) & \mathbf{A}_2(\mathbf{w}_2) & -\mathbf{S}_2(\mathbf{w}_2) & 0 & -\mathbf{S}_4(\mathbf{w}_2) \\ 0 & 0 & 0 & 0 & 0 \\ 0 & 0 & 0 & 0 & 0 \\ 0 & 0 & 0 & 0 & 0 \end{pmatrix},$$

$$\mathbf{S}_1(\mathbf{w}_i) = \begin{pmatrix} 0 \\ -gh_i \\ 0 \end{pmatrix}, \mathbf{S}_2(\mathbf{w}_i) = \begin{pmatrix} 0 \\ 0 \\ -gh_i \end{pmatrix}, \mathbf{S}_3(\mathbf{w}_i) = \begin{pmatrix} 0 \\ fh_i v_i \\ 0 \end{pmatrix}, \mathbf{S}_4(\mathbf{w}_i) = \begin{pmatrix} 0 \\ 0 \\ -fh_i u_i \end{pmatrix}.$$

Further, $\mathbf{A}_1$, $\mathbf{A}_2$ are the usual Jacobian matrices of conservative fluxes in $x-, y-$ directions, respectively, and $\mathbf{C}_1, \mathbf{C}_2, \widetilde{\mathbf{C}}_1, \widetilde{\mathbf{C}}_2$ the corresponding coupling matrices containing the non-conservative terms. For example, we have

$$\mathbf{C}_1(\mathbf{w}_1) = \begin{pmatrix} 0 & 0 & 0 \\ c_1^2 & 0 & 0 \\ 0 & 0 & 0 \end{pmatrix}, \qquad \widetilde{\mathbf{C}}_2(\mathbf{w}_2) = \begin{pmatrix} 0 & 0 & 0 \\ 0 & 0 & 0 \\ rc_2^2 & 0 & 0 \end{pmatrix}.$$

The difficulty of the two-layer system lies in the coupling matrices $\mathbf{C}_i, \widetilde{\mathbf{C}}_i$. Indeed, the matrix pencil

$$\begin{pmatrix} \mathbf{A}_1(\mathbf{w}_1) & \mathbf{C}_1(\mathbf{w}_1) \\ \widetilde{\mathbf{C}}_1(\mathbf{w}_2) & \mathbf{A}_1(\mathbf{w}_2) \end{pmatrix} \cos\theta + \begin{pmatrix} \mathbf{A}_2(\mathbf{w}_1) & \mathbf{C}_2(\mathbf{w}_1) \\ \widetilde{\mathbf{C}}_2(\mathbf{w}_2) & \mathbf{A}_2(\mathbf{w}_2) \end{pmatrix} \sin\theta, \qquad \theta \in (0, 2\pi)$$

may have complex eingenvalues and the hyperbolicity of the system is lost. Even if we would be able to approximate eigenvalues at least in the case when they are real it is too expensive to construct the corresponding eigenvectors. The latter are however necessary in order to apply the characteristic (or bicharacteristic) decomposition needed for the evolution operator in the predictor step of the FVEG scheme. These considerations lead us to a construction of a suitable decomposition of the system (4) into a set of subsystems for which the corresponding eigenstructure is readily available. In the present paper we apply a natural operator splitting that sep-

arates each layer, see also [2] for similar approach. Note however, that other splitting techniques are possible [7] and will be reported in our future work.

In what follows the following decomposition will be used:
operator T^1

$$\begin{aligned}&\partial_t \mathbf{w}_1 + \mathbf{A}_1(\mathbf{w}_1)\partial_x \mathbf{w}_1 + \mathbf{A}_2(\mathbf{w}_1)\partial_y \mathbf{w}_1 = \\ &-\mathbf{C}_1(\mathbf{w}_1)\partial_x \mathbf{w}_2 - \mathbf{C}_2(\mathbf{w}_1)\partial_y \mathbf{w}_2 + \mathbf{S}_1(\mathbf{w}_1)\partial_x b + \mathbf{S}_2(\mathbf{w}_1)\partial_y b + \mathbf{S}_3(\mathbf{w}_1) + \mathbf{S}_4(\mathbf{w}_1)\end{aligned} \tag{5}$$

operator T^2

$$\begin{aligned}&\partial_t \mathbf{w}_2 + \mathbf{A}_1(\mathbf{w}_2)\partial_x \mathbf{w}_2 + \mathbf{A}_2(\mathbf{w}_2)\partial_y \mathbf{w}_2 = \\ &-\widetilde{\mathbf{C}}_1(\mathbf{w}_2)\partial_x \mathbf{w}_1 - \widetilde{\mathbf{C}}_2(\mathbf{w}_2)\partial_y \mathbf{w}_1 + \mathbf{S}_1(\mathbf{w}_2)\partial_x b + \mathbf{S}_2(\mathbf{w}_2)\partial_y b + \mathbf{S}_3(\mathbf{w}_2) + \mathbf{S}_4(\mathbf{w}_2)\end{aligned} \tag{6}$$

Thus, instead of solving a complex system (4) the second order Strang splitting approach is applied using the operators T^1 and T^2

$$\mathbf{W}^{n+1} = T^1_{\Delta t/2} T^2_{\Delta t} T^1_{\Delta t/2} \mathbf{W}^n. \tag{7}$$

Note that the operators T^1, T^2 can be easily rewritten in the form (4) by setting, respectively, the second and first row in the matrices $\widetilde{\mathbf{A}}_1$ and $\widetilde{\mathbf{A}}_2$ to zero. In fact, we have for the operator T^1

$$\mathbf{W}_t + \widetilde{\mathbf{A}}^1_1(\mathbf{W})\mathbf{W}_x + \widetilde{\mathbf{A}}^1_2(\mathbf{W})\mathbf{W}_y = 0,$$

$$\widetilde{\mathbf{A}}^1_1 = \begin{pmatrix} \mathbf{A}_1(\mathbf{w}_1) & \mathbf{C}_1(\mathbf{w}_1) & -\mathbf{S}_1(\mathbf{w}_1) & -\mathbf{S}_3(\mathbf{w}_1) & 0 \\ 0 & 0 & 0 & 0 & 0 \\ 0 & 0 & 0 & 0 & 0 \\ 0 & 0 & 0 & 0 & 0 \\ 0 & 0 & 0 & 0 & 0 \end{pmatrix}$$

$$\widetilde{\mathbf{A}}^1_2 = \begin{pmatrix} \mathbf{A}_2(\mathbf{w}_1) & \mathbf{C}_2(\mathbf{w}_1) & -\mathbf{S}_2(\mathbf{w}_1) & 0 & -\mathbf{S}_4(\mathbf{w}_1) \\ 0 & 0 & 0 & 0 & 0 \\ 0 & 0 & 0 & 0 & 0 \\ 0 & 0 & 0 & 0 & 0 \\ 0 & 0 & 0 & 0 & 0 \end{pmatrix}.$$

The analogous equations hold for the operator T^2. Clearly, each system (5), (6) now reduces to the one-layer shallow water equations with a generalized bottom topography $h_2 + b$ or $rh_1 + b$. These are known for a given time step using the values from the previous time step. Our next aim is to derive a *well-balanced path-consistent FVEG scheme* for each layer separately.

3 Path-consistent FVEG scheme

Let us discretize a computational domain Ω by a regular rectangular mesh consisting of finite volumes $\Omega_{k\ell} = (x_k - \hbar/2, x_k + \hbar/2) \times (y_\ell - \hbar/2, y_\ell + \hbar/2)$, $k, \ell \in \mathbb{Z}$ and denote by $\hbar$ the mesh step and by Δt time step. For each layer the path-consistent FVEG scheme is a predictor-corrector method. The corrector step is a path-consistent FV update, in the predictor step an intermediate solution $\mathbf{W}^*$ on cell interfaces and cell centers is computed using an approximate evolution operator for the related layer, cf. Section 4.

In order to derive a path-consistent FV update we need to construct a suitable path in the phase space

$$\tilde{\Phi}(s, \mathbf{W}^*_{k,\ell'}, \mathbf{W}^*_{k+1,\ell'}) := \begin{cases} \Phi(2s, \mathbf{W}^*_{k,\ell'}, \mathbf{W}^*_{k+1/2,\ell'}) & 0 \le s \le 1/2, \\ \Phi(2s-1, \mathbf{W}^*_{k+1/2,\ell'}, \mathbf{W}^*_{k+1,\ell'}) & 1/2 \le s \le 1, \end{cases}$$

here $\Phi(s, \mathbf{W}^*_a, \mathbf{W}^*_b)$ is a straight path connecting $\mathbf{W}^*_a$ and $\mathbf{W}^*_b$, $\mathbf{W}^*$ is obtained by the evolution Galerkin operator in the predictor step.

The path-consistent finite volume update reads for each operator T^i, $i = 1, 2$

$$\begin{aligned} \mathbf{W}^{new}_{k,\ell} = \mathbf{W}^{old}_{k,\ell} &- \frac{\tau}{\hbar} \sum_{\ell' \in L} \alpha_{\ell'} \left(\mathbf{D}^{i,-}_{k+1/2,\ell'} + \mathbf{D}^{i,+}_{k-1/2,\ell'} \right) \\ &- \frac{\tau}{\hbar} \sum_{k' \in K} \beta_{k'} \left(\mathbf{D}^{i,-}_{k',\ell+1/2} + \mathbf{D}^{i,+}_{k',\ell-1/2} \right), \end{aligned} \tag{8}$$

where $\tau = \Delta t$ or $\tau = \Delta t/2$, $L := \{\ell - 1/2, \ell, \ell + 1/2\}$ and $K := \{k - 1/2, k, k + 1/2\}$ are the index sets and $\alpha_{\ell'}$, $\beta_{k'}$ the weights of the Simpson quadrature applied for flux integration along cell interfaces. Now let us define the $\mathbf{D}$ matrices for each $k, \ell \in \mathbb{Z}, k' \in K, \ell' \in L$

$$\mathbf{D}^{i,-}_{k+1/2,\ell'} := \int_0^1 \widetilde{\mathbf{A}}^i_1(\Phi(s; \mathbf{W}^*_{k,\ell'}, \mathbf{W}^*_{k+1/2,\ell'})) \frac{\partial \Phi}{\partial s}(s; \mathbf{W}^*_{k,\ell'}, \mathbf{W}^*_{k+1/2,\ell'})\, ds, \tag{9}$$

$$\mathbf{D}^{i,+}_{k+1/2,\ell'} := \int_0^1 \widetilde{\mathbf{A}}^i_1(\Phi(s; \mathbf{W}^*_{k+1/2,\ell'}, \mathbf{W}^*_{k+1,\ell'})) \frac{\partial \Phi}{\partial s}(s; \mathbf{W}^*_{k+1/2,\ell'}, \mathbf{W}^*_{k,\ell'})\, ds, \tag{10}$$

matrices $\mathbf{D}^{i,+}_{k',\ell+1/2}, \mathbf{D}^{i,-}_{k',\ell+1/2}$ are defined using $\widetilde{\mathbf{A}}^i_2$ in an analogous way, $i = 1, 2$.

After a short calculation we obtain for each layer, $i = 1, 2$, the following representation of source terms

$$(\mathbf{S}_1(\mathbf{w}_i^*)\partial_x b)_{k+1/2,\ell'} =$$
$$\frac{g}{2}\begin{pmatrix} 0 \\ ((h_i^*)_{k,\ell'}+(h_i^*)_{k+1/2,\ell'})(b^*_{k,\ell'}-b^*_{k+1/2,\ell'})+((h_i^*)_{k-1/2,\ell'}+(h_i^*)_{k,\ell'})(b^*_{k-1/2,\ell'}-b^*_{k,\ell'}) \\ 0 \end{pmatrix},$$
$$(\mathbf{S}_2(\mathbf{w}_i^*)\partial_y b)_{k',\ell+1/2} =$$
$$\frac{g}{2}\begin{pmatrix} 0 \\ 0 \\ ((h_i^*)_{k',\ell}+(h_i^*)_{k',\ell+1/2})(b^*_{k',\ell'}-b^*_{k',\ell+1/2})+((h_i^*)_{k',\ell-1/2}+(h_i^*)_{k',\ell})(b^*_{k',\ell-1/2}-b^*_{k',\ell}) \end{pmatrix},$$
$$(\mathbf{S}_3(\mathbf{w}_i^*)\partial_x x)_{k+1/2,\ell'} =$$
$$f\frac{\hbar}{4}\begin{pmatrix} 0 \\ (h_i^*)_{k-1/2,\ell'}(v_i^*)_{k-1/2,\ell'}+2(h_i^*)_{k,\ell'}(v_i^*)_{k,\ell'}+(h_i^*)_{k+1/2,\ell'}(v_i^*)_{k+1/2,\ell'} \\ 0 \end{pmatrix},$$

$$(\mathbf{S}_4(\mathbf{w}_i^*)\partial_y y)_{k',\ell+1/2} =$$
$$-f\frac{\hbar}{4}\begin{pmatrix} 0 \\ 0 \\ (h_i^*)_{k',\ell-1/2}(u_i^*)_{k',\ell-1/2}+2(h_i^*)_{k',\ell}(u_i^*)_{k',\ell}+(h_i^*)_{k',\ell+1/2}(u_i^*)_{k',\ell+1/2} \end{pmatrix}.$$

Let us point out that the discretization of source terms obtained above using the path-consistent approach and those derived in [10] are different. Nevertheless both approaches yield well-balanced approximations, cf. [10] and Theorem 1 below.

4 Approximate evolution operators

In order to keep the paper self-contained we present the first order approximate evolution operator T^1, the approximate evolution operator T^2 can be written in an analogous way. For the second order version and for the detailed derivation of approximate evolution operators the reader is referred to [10]. The approximate evolution operator $\mathbf{W}^* = EG^1_{\tau/2}\mathbf{W}^{old}$ for the operator T^1_τ reads

$$h_1(P) = -b(P) - h_2(P) +$$
$$\frac{1}{2\pi}\int_0^{2\pi}\left[(h_1(Q)+b(Q)+h_2(Q)) - \frac{\tilde{c_1}}{g}(u_1(Q)\operatorname{sgn}(\cos\theta)+v_1(Q)\operatorname{sgn}(\sin\theta))\right]\mathrm{d}\theta$$
$$+\frac{\tau}{4\pi}\int_0^{2\pi}(\tilde{u}_1(b_x(Q)+(h_2)_x(Q))+\tilde{v}_1(b_y(Q)+(h_2)_y(Q)))\,\mathrm{d}\theta$$

$$u_1(P) = \frac{1}{2\pi}\int_0^{2\pi}\Big[-\frac{1}{\tilde{c_1}}K_1(Q)\,\mathrm{sgn}(\cos\theta) + u_1(Q)\left(\cos^2\theta+\frac{1}{2}\right) + v_1(Q)\sin\theta\cos\theta\Big]\mathrm{d}\theta$$

$$v_1(P) = \frac{1}{2\pi}\int_0^{2\pi}\Big[-\frac{1}{\tilde{c_1}}L_1(Q)\,\mathrm{sgn}(\sin\theta) + u_1(Q)\sin\theta\cos\theta + v_1(Q)\left(\sin^2\theta+\frac{1}{2}\right)\Big]\mathrm{d}\theta$$

$$h_2(P) = \frac{1}{2\pi}\int_0^{2\pi} h_2(Q)\,\mathrm{d}\theta, \quad b(P) = \frac{1}{2\pi}\int_0^{2\pi} b(Q)\,\mathrm{d}\theta \tag{11}$$

$$u_2(P) = \frac{1}{2\pi}\int_0^{2\pi} u_2(Q)\,\mathrm{d}\theta, \quad v_2(P) = \frac{1}{2\pi}\int_0^{2\pi} v_2(Q)\,\mathrm{d}\theta$$

Here $\tau = \Delta t/2$, due to the Strang splitting (7) we have $\tau = \Delta t$ for the T^2 operator. Further, K_1 and L_1 are the potential energies in the $x-$ and $y-$ directions defined as $K_1 := g(h_1+h_2+b-V_1)$, $L_1 := g(h_1+h_2+b+U_1)$, where V_1, U_1 are the primitives to the Coriolis forces, i.e. $\partial_x(V_1) = \frac{f}{g}v_1$, $\partial_y(U_1) = \frac{f}{g}u_1$. In the equations (11) the evolution takes place along the so-called bicharacteristic cone having the peak at $P = (x, y, t^{old}+\tau/2)$ and footpoints Q on the sonic circle, i.e. $Q = (x-\tilde{u}_1\tau/2-\tilde{c}_1\tau/2\cos\theta, y-\tilde{v}_1\tau/2-\tilde{c}_1\tau/2\sin\theta, t^{old})$, $\theta\in(0,2\pi)$; $\tilde{u}_1, \tilde{v}_1, \tilde{c}_1$ are the constant states obtained by a local linearization (e.g. local averaging).

5 Well-balancing of the path-consistent FVEG scheme

The aim of this section is to verify the well-balanced property of the path-consistent FVEG scheme (7), (8).

Theorem 1. *Suppose that the solution at time t^n satisfy for all (x,y) the equilibrium conditions (2) and (3). Then the path-consistent FVEG scheme satisfies the same well-balanced conditions for the new time level t^{n+1}. More precisely, the rest at state condition (2) is preserved exactly and the geostrophic equilibrium condition (3) is satisfied for smooth solutions up to at least third order accuracy.*

Proof. i) First, it is clear that if the operators T^1 and T^2 are well-balanced the complete path-consistent scheme (7) will be well-balanced as well.

Further, we have shown in [10] that the approximate evolution operator (11) satisfies these conditions exactly for the corresponding generalized bottom topography h_2+b; the same is true for the second layer with the generalized topography rh_1+b.

Thus for each layer, the predicted solutions $\mathbf{W}^*$ satisfy the above conditions (2), (3) exactly.

ii) Now, we need to show that the finite volume update (8) preserves these conditions as well. We will first consider the rest state conditions: using $u_i^* = 0$, $v_i^* = 0$, for $i = 1,2$, and $h_1^*+h_2^*+b = c_1$, $rh_1^*+h_2^*+b = c_2$, $c_1 = \text{const.}$, $c_2 = \text{const.}$ we get

for the first layer for each k,ℓ

$$(h_1)^{new}_{k,\ell} = (h_1)^{old}_{k,\ell}$$

$$\begin{aligned}(h_1u_1)^{new}_{k,\ell} = -\frac{\Delta t}{\hbar}\sum_{\ell'\in L}\alpha_{\ell'}\frac{g}{2}\Big[&\Big((h_1^*)^2_{k+1/2,\ell'} - (h_1^*)^2_{k-1/2,\ell'}\Big)\\ &+\Big((h_1^*)_{k-1/2,\ell'} + (h_1^*)_{k,\ell'}\Big)\Big(B^*_{k,\ell'} - B^*_{k-1/2,\ell'}\Big)\\ &+\Big((h_1^*)_{k+1/2,\ell'} + (h_1^*)_{k,\ell'}\Big)\Big(B^*_{k+1/2,\ell'} - B^*_{k,\ell'}\Big)\Big],\end{aligned} \tag{12}$$

where we set $B = b + h_2$. Now we have on the right hand side of (12)

$$\begin{aligned}&(h_1^*)^2_{k+1/2,\ell'} - (h_1^*)^2_{k-1/2,\ell'} + \Big((h_1^*)_{k-1/2,\ell'} + (h_1^*)^2_{k,\ell'}\Big)\Big(B^*_{k,\ell'} - B_{k-1/2,\ell'}\Big)\\ &\qquad + \Big((h_1^*)_{k+1/2,\ell'} + (h_1^*)_{k,\ell'}\Big)\Big(B^*_{k+1/2,\ell'} - B^*_{k,\ell'}\Big)\\ =\ &(h_1^*)_{k+1/2,\ell'}c_1 - (h_1^*)_{k-1/2,\ell'}c_1 + \Big((h_1^*)_{k-1/2,\ell'} - (h_1^*)_{k+1/2,\ell'}\Big)B^*_{k,\ell'}\\ &\qquad + (h_1^*)_{k,\ell'}\Big(B^*_{k+1/2,\ell'} - B^*_{k-1/2,\ell'}\Big)\\ =\ &\Big((h_1^*)_{k+1/2,\ell'} - (h_1^*)_{k-1/2,\ell'}\Big)\Big(c_1 - B^*_{k,\ell'}\Big) + (h_1^*)_{k,\ell'}\Big(B^*_{k+1/2,\ell'} - B^*_{k-1/2,\ell'}\Big)\\ =\ &(h_1^*)_{k,\ell'}(c_1 - c_1) = 0.\end{aligned}$$

The analogous equations hold for the momentum equation in the y-direction. Altogether these imply that $h_1^{new} = h_1^{old}$, $u_1^{new} = 0 = v_1^{new}$. The same relations hold analogously for the second layer $h_2^{new} = h_2^{old}$, $u_2^{new} = 0 = v_2^{new}$, so that together with the results from *i)* we have $h_1^{n+1} + h_2^{n+1} + b = c_1$ and $rh_1^{n+1} + h_2^{n+1} + b = c_2$.

iii) The proof for the geostrophic equilibrium (3) is analogous. The first equation for the conservation of momentum yields $(h_1)^{n+1}_{k\ell} = 0$ and $(h_2)^{n+1}_{k\ell} = 0$. However, the momentum equation in the $x-$ direction yields only $u_i^{n+1} = \mathscr{O}(\hbar^3), \quad i = 1,2$. Indeed,

$$\begin{aligned}(h_1u_1)^{new}_{k\ell} = -\frac{\Delta t}{\hbar}\sum_{\ell'\in L}\alpha_{\ell'}\Big[&\frac{g}{2}\Big((h_1^*)^2_{k+1/2,\ell'} - (h_1^*)^2_{k-1/2,\ell'}\Big)\\ +f\frac{\hbar}{4}\quad&\Big((h_1^*)_{k-1/2,\ell'}(v_1^*)_{k-1/2,\ell'} + 2(h_1^*)_{k\ell'}(v_1^*)_{k\ell'} + (h_1^*)_{k+1/2,\ell'}(v_1^*)_{k+1/2,\ell'}\Big)\Big] =\\ -\frac{\Delta t}{\hbar}\quad&\sum_{\ell'\in L}\alpha_{\ell'}\Big[\frac{g}{2}\Big((h_1^*)_{k+1/2,\ell'} + (h_1^*)_{k-1/2,\ell'}\Big)\Big((K_1^*)_{k+1/2,\ell'} - (K_1^*)_{k-1/2,\ell'}\Big) + \mathscr{E}\Big],\end{aligned} \tag{13}$$

here $\mathscr{E}$ is the error term and K_1 is the potential energy, thus setting for simplicity of the presentation $K_1 = h_1 + V_1$. Then $(K_1^*)_{k+1/2,\ell'} - (K_1^*)_{k-1/2,\ell'} = (h_1^*)_{k+1/2,\ell'} - (h_1^*)_{k-1/2,\ell'} + f\frac{\hbar}{2}((v_1^*)_{k+1/2,\ell'} + (v_1^*)_{k-1/2,\ell'}) = 0$. The error term gives

$$\mathscr{E} = \frac{f\hbar}{4}\left((h_1^*)_{k+1/2,\ell'}(v_1^*)_{k-1/2,\ell'} + (h_1^*)_{k-1/2,\ell'}(v_1^*)_{k+1/2,\ell'} - 2(h_1^*)_{k,\ell'}(v_1^*)_{k,\ell'}\right) = \mathscr{O}(\hbar^3),$$

which together with an analogous equation for the second layer concludes the proof.

6 Numerical experiments

In this section we want to demonstrate the behaviour of new path-consistent FVEG scheme through some numerical experiments.

Problem 1

First, we test accuracy of the path-consistent FVEG scheme. The initial data are as follows

$$\begin{aligned} b(x,y) &= -\frac{1}{2}\exp(\sin^2(\pi x)),\\ h_1(0,x,y) &= 5+\exp(\cos(2\pi x)),\\ h_2(0,x,y) &= 5+\sin^2(\pi x)-b(x),\\ u_1(0,x,y) &= \sin(\cos(2\pi x))/h_1(x,0)\\ u_2(0,x,y) &= 0. \end{aligned}$$

We apply periodic boundary conditions and set $r = 0.98$, $g = 9.812$. The computational domain $[0,1]\times[0,1]$ is divided into $N\times N$ mesh cells, $N = 20,\ldots,160$. In the following table we present behaviour of the relative global L^1 error of the second order well-balanced path-consistent FVEG scheme. The solution was computed until $T = 0.1$ and no limiter has been used in this experiment. The CFL number is chosen to be $CFL = 0.9$.

	FVEG			
N	h_1	EOC	h_2	EOC
20	2.31e-03		1.45e-03	
40	4.28e-04	2.43	4.02e-04	1.85
80	7.73e-05	2.47	8.36e-05	2.27
160	1.59e-05	2.28	1.92e-05	2.12

	FVEG			
N	q_1	EOC	q_2	EOC
20	6.87e-02		9.48e-02	
40	1.32e-02	2.39	1.97e-02	2.27
80	2.29e-03	2.52	3.70e-03	2.41
160	4.61e-04	2.32	7.82e-04	2.24

Table 1 L_1 errors of the well-balanced path-consistent FVEG method

Table 1 clearly demonstrates the second order accuracy of the FVEG method. Interestingly, we can notice very accurate behaviour of our path-consistent FVEG scheme, for example, in comparison with the well-balanced higher order FV WENO scheme that uses fourth order Runge-Kutta method for time evolution. The latter has been developed by Frings in [5].

Problem 2

This is an internal dam-break problem. We have imposed initially a jump at the interface, while still having the total water height constant.

$$h_1(0,x) = \begin{cases} 0.2, & \text{if } x < 5, \\ 1.8, & \text{if } x > 5, \end{cases}$$
$$h_2(0,x) = \begin{cases} 1.8, & \text{if } x < 5, \\ 0.2, & \text{if } x > 5, \end{cases}$$
$$u_1(0,x) = u_2(0,x) = 0,\ b(x) = 0, \qquad x \in (0,10).$$

In the following figures solution obtained by the path-consistent second order FVEG scheme for the case $r = 0.7$ at time $t = 0.1$ and $r = 0.98$ at $t = 5$ is plotted, see Figures 2,3. We can nicely recognize the structure of the solution consisting of three constant states connected by two rarefaction waves and two shocks. No oscillations or smearing of shocks can be seen, that was a problem reported by other authors, cf. [2]. The minmod limiter has been used in the second order reconstruction.

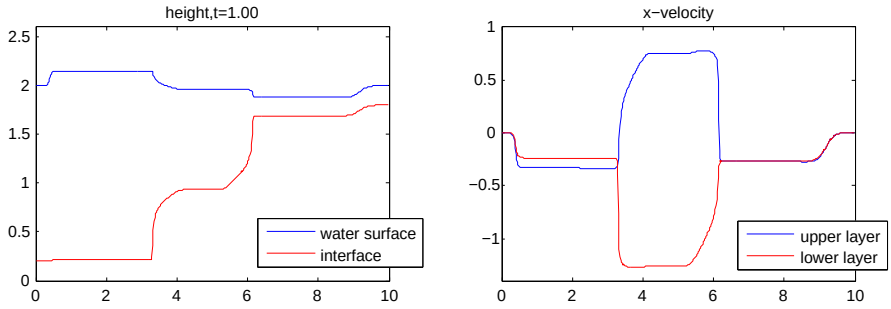

Fig. 2 Solution obtained by the path-consistent FVEG scheme at time $t = 1.0$, $\frac{\rho_1}{\rho_2} = 0.7$

Problem 3

The last problem is a geostrophic adjustment simulation for two-layer shallow water model, analogous problem for the one-layer shallow water has been considered in [6]. The initial conditions are

$$h_1(x,y,0) = 1 + \frac{A_0}{2}\left(1 - \tanh\left(\frac{\sqrt{(\sqrt{\lambda}x)^2 + (y/\sqrt{\lambda})^2} - R_i}{R_E}\right)\right),$$
$$h_2(x,y,0) = 1, \quad u_1(x,y,0) = v_1(x,y,0) = u_2(x,y,0) = v_2(x,y,0) = 0,$$

where the parameters are $A_0 = 0.5$, $\lambda = 2.5$, $R_E = 0.1$, and $R_i = 1$. The gravity and the Coriolis forces parameters are set to $g = 1$, $f = 1$, fraction of layers density is $r = 0.98$. No bottom topography is considered. The computational domain

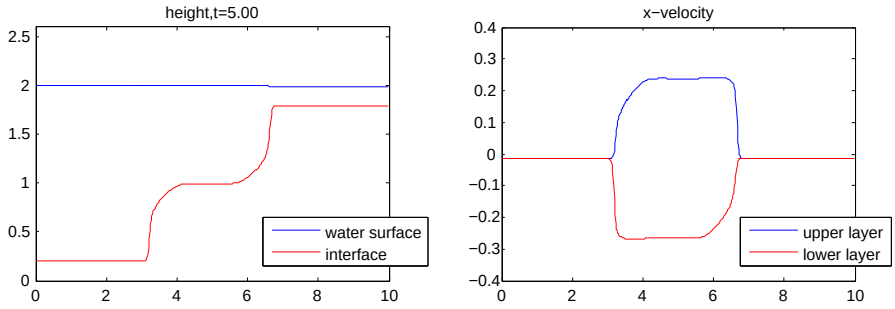

Fig. 3 Solution obtained by the path-consistent FVEG scheme at time $t = 5.0$, $\frac{\rho_1}{\rho_2} = 0.98$

$[-10,10] \times [-10,10]$ has been divided into 400×400 mesh cells. The CFL number was set to 0.6. In Figure 4 we see results of time evolution of initial perturbation of top surface. Results were obtained by the second order path-consistent FVEG scheme using bilinear recovery with minmod limiter. Two circular shock waves propagating in the top surface $h_1 + h_2$ and in the second layer h_2 can be recognized nicely. Behind the shocks there is elevation rotating anti-clockwise. In order to represent absorbing boundary conditions extrapolation has been implemented on the boundary of computational domain.

Acknowledgements

The present research has been partially supported by the Deutsche Forschungsgemeinschaft under the grant LU 1470/2-1 and by the European Graduate School Differential Equations with Applications in Science and Engineering (DEASE), MEST-CT-2005-021122.

References

1. Abgrall R., Karni S.: Two–layer shallow water systems: a relaxation approach. SIAM J. Sci. Comput **31(3)** 1603–1627 (2009)
2. Bouchut F., Morales T.: An entropy satisfying scheme for two-layer shallow water equations with uncoupled treatment. M2AN **42** 683–698 (2008)
3. Dal Maso G., LeFloch P.G., Murat F.: Definition and weak stability of nonconservative products. J. Math. Pures Appl. **74**, 483-548 (1995)
4. Castro M.J., LeFloch P.G., Munoz-Ruiz M.L., Parés C.: Why many theories of shock waves are necessary. Convergence error in formally path-consistent schemes. J. Comp. Phys. (2008)
5. Frings J.: Well-Balanced Finite Volumes of Higher Order of Accuracy for Two-Layer Shallow Water Flows. Master Thesis, RWTH Aachen (2007)

6. Castro M.J., López J.A., Parés C.: Finite volume simulation of the geostrophic adjustment in a rotating shallow-water system. SIAM J. Sci. Comput. **31**, 444–477 (2008)
7. Kurganov A., Petrova G.: Central-upwind schemes for two-layer shallow water equations. SIAM J. Sci. Comput. **31**, 1742–1773 (2009)
8. Lukáčová-Medviďová M., Morton K.W., Warnecke G.: Finite volume evolution Galerkin (FVEG) methods for hyperbolic problems. SIAM J. Sci. Comput. **26(1)**, 1–30 (2004)
9. Lukáčová-Medviďová M., Vlk Z.: Well-balanced Finite Volume Evolution Galerkin Methods for the Shallow Water Equations with Source Terms. Int. J. Num. Fluids. **47(10-11)**, 1165–1171 (2005)
10. Lukáčová-Medviďová M., Noelle S., Kraft M.: Well-balanced finite volume evolution Galerkin methods for the shallow water equations. J. Comp. Phys. **221**, 122–147 (2007)
11. Parés C.: Numerical methods for nonconservative hyperbolic systems: a theoretical framework. SIAM J. Numer. Anal. **44**, 300-321 (2006)
12. Parés C., Castro M.J.: On the well-balance property of Roes method for nonconservative hyperbolic systems. Applications to shallow-water systems. Math. Model. Numer. Anal. **38**, 821-852 (2004)

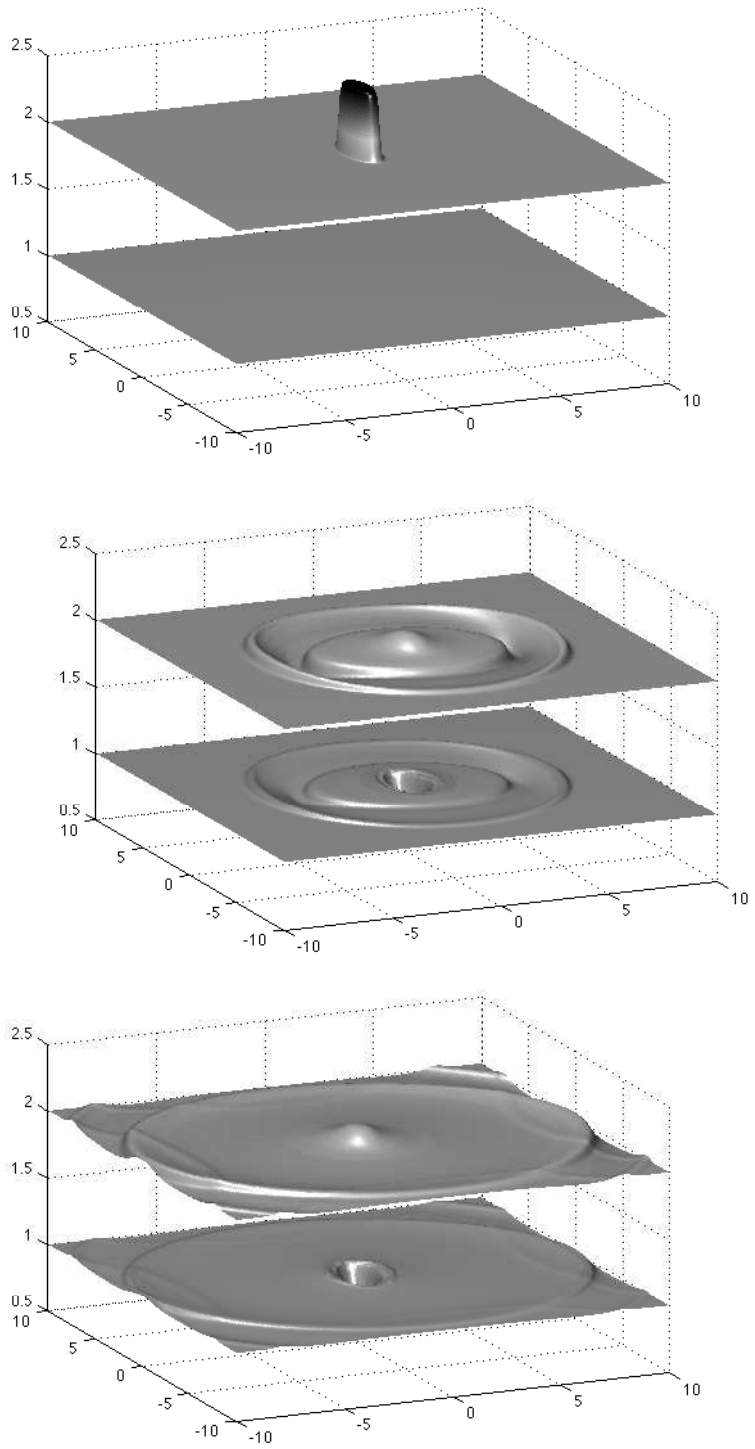
2.5
2
1.5
1
0.5
10
5
0
-5
-10
-10
-5
0
5
10

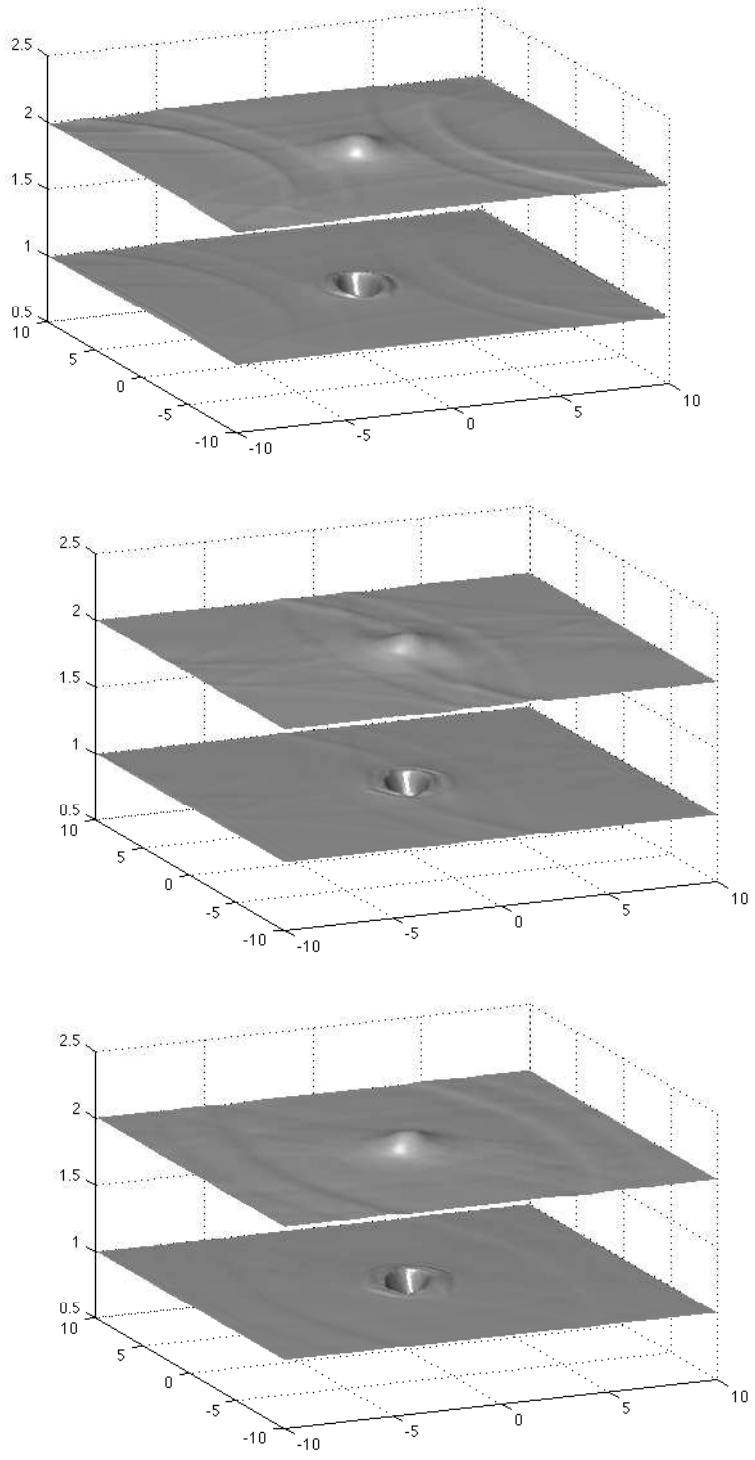

Fig. 4 Effects of Coriolis forces in the two-layer model at $t = 0, 4, 8, 12, 16, 20$